



**HAL**  
open science

# Long-term behavior of salt caverns in the Matacães solution mining concession in Portugal: in-situ measurements and numerical modeling

Alain Thoraval, Xavier Daupley, Franz Lahaie, Thomas Richard, Paulo Quental

► **To cite this version:**

Alain Thoraval, Xavier Daupley, Franz Lahaie, Thomas Richard, Paulo Quental. Long-term behavior of salt caverns in the Matacães solution mining concession in Portugal: in-situ measurements and numerical modeling. SMRI Fall Technical Conference 2018, Sep 2018, Belfast, United Kingdom. ineris-03239663

**HAL Id: ineris-03239663**

**<https://ineris.hal.science/ineris-03239663>**

Submitted on 27 May 2021

**HAL** is a multi-disciplinary open access archive for the deposit and dissemination of scientific research documents, whether they are published or not. The documents may come from teaching and research institutions in France or abroad, or from public or private research centers.

L'archive ouverte pluridisciplinaire **HAL**, est destinée au dépôt et à la diffusion de documents scientifiques de niveau recherche, publiés ou non, émanant des établissements d'enseignement et de recherche français ou étrangers, des laboratoires publics ou privés.

# Long-term behavior of salt caverns in the Matacães solution mining concession in Portugal – In situ measurements and numerical modeling

Alain Thoraval, Xavier Daupley, Franz Lahaie, Thomas Richard,  
Ineris – Institut National de l'Environnement et des Risques, France

Paulo Quental, Solvay, Brussels, Belgium

## Abstract

Since 1954, the Solvay company has operated, by isolated caverns, a salt dome in the Matacães concession in Portugal (Torres Vedras region, 40 km north of Lisbon). A total of 22 caverns were created for a production of nearly 19 million tons of salt in 60 years. In a perspective of securing the cavern before final closure, Solvay asked Ineris to deepen knowledge of their current conditions and to predict evolutions before and after their closure. To this end, numerical modeling was implemented, based on field measurements and tests (thermography, volumetry, brine purges, creep tests).

The analysis of purges first enabled an evaluation of the compressibility factor of the caverns and the identification of possible hydraulic communications between caverns. The analysis of the temperature profiles led to distinguishing caverns that are already at thermal equilibrium and those that are not. Finally, the salt creep parameters were estimated from the pressure rise measurements between 2 purges and the well discharge measurements obtained during the creep tests. The results show a certain variability of creep parameters, probably reflecting a certain heterogeneity of the salt dome.

2D-axi models show that the current state of mechanical stability of caverns is not of concern as no critical zones were identified. The simulation of the long-term evolution after well plugging highlights the absence of critical evolution for most caverns. However, for some caverns, a risk of roof failure was characterized by the fact that the brine pressure locally becomes larger than the lithostatic stress. The most critical situations are obtained for the most elongated or highly thermally unbalanced caverns.

The simulations carried out have highlighted the high sensitivity of the results to the value of salt permeability and to the waiting time before well plugging. It appears that the lower the salt permeability, the greater the pressure peak and the risk of salt failure at the roof of the cavern. Moreover, the increase in waiting time before well plugging reduces the thermal imbalance, and therefore the value of the maximum pressure in the cavern. It therefore leads to a reduction in the risk of failure. It remains to specify the value of the permeability and then the conditions of closure for the most critical caverns. An abandonment test is planned soon to help in this purpose.

**Key words:** post-mining, salt caverns, in situ measurements, numerical modeling.

## 1. Introduction

Since 1954, the Solvay company has operated, by isolated caverns, a salt diapir in the Matacães concession in Portugal (Torres Vedras region, 40 km north of Lisbon). Solvay asked Ineris to serve as a scientific and technical consultant during different post-operation site-monitoring stages. Analysis of the caverns' and access wells' stability conditions in the short, medium and long term is part of Ineris's mission. To do so, numerical modeling was implemented, based on operations data, recent field measurements and tests (thermography, volumetry, purges, creep tests).

### a. Geological context

The Matacães region is in the Central Lusitanian Basin. During the Jurassic period, the Lusitanian Basin was subjected to several rifts related to the opening of the North Atlantic Ocean. During this era, certain halokinetic phenomena were triggered (rising of the Dagorda Formation toward the surface). The Dagorda salt formation dates from the end of the Triassic and Hettangian periods (lower Jurassic).

The Matacães salt diapir operated by Solvay corresponds to the surface outcropping of the Dagorda Formation, which contains the salt deposit. Diapirism induced the formation of an anticlinal geological structure with an east-west axis. The first hundred meters of this formation, close to the surface, have been virtually emptied of their salt. The deposit's beds have been reached at a depth between 170 and 490 meters, depending on the surface location and the considered well, but also the salt content under consideration. The diapir's sidewalls are made up of limestone, marl and sandstone formations, pierced and raised by diapirism.

### b. Characteristics of the operation

The salt deposit was operated through the creation of isolated dissolution caverns between 1957 and 2014, when salt production ended. 28 caverns were created from 22 wells, spread out over two sites: Matacães 1 (18 caverns from 15 wells) and Matacães 2 (10 caverns from 7 wells). The principal characteristics are given in **Table 1**.

**Table 1.** Principal characteristics of the caverns at the Matacães site

| Well              | Activity period |      | Roof depth (m) | Cavern height h (m) | Cavern volume V (m <sup>3</sup> ) | Average radius (V/πh) <sup>1/2</sup> |
|-------------------|-----------------|------|----------------|---------------------|-----------------------------------|--------------------------------------|
|                   | start           | end  |                |                     |                                   |                                      |
| <b>Matacães 1</b> |                 |      |                |                     |                                   |                                      |
| Sag 3             | 1957            | 1980 | 303 and 491    | 174.5 + 169         | 327000                            | 17.4                                 |
| Sag 4             | 1957            | 1975 | 432            | 60                  | 79000                             | 20.5                                 |
| Sag 5             | 1957            | 1974 | 390            | 106                 | 177000                            | 23.1                                 |
| Sag 6             | 1960            | 1989 | 300            | 398.75              | 500000                            | 20                                   |
| Sag 7             | 1970            | 1990 | 289            | 366                 | 428000                            | 19.3                                 |
| Sag 8             | 1971            | 1980 | 332            | 339                 | 279000                            | 16.2                                 |
| Sag 9             | 1971            | 1993 | 400            | 386                 | 426000                            | 18.75                                |
| Sag 10            | 1977            | 2002 | 630            | 224.40              | 474000                            | 25.9                                 |
| Sag 11            | 1977            | 1978 | 823            | 53                  | 15000                             | 9.5                                  |
| Sag 12            | 1978            | 2008 | 326 and 644    | 184 + 96            | 370000                            | 20.5                                 |
| Sag 13            | 1980            | 2014 | 540            | 364.15              | 810000                            | 26.6                                 |
| Sag 14            | 1979            | 2014 | 548            | 334.95              | 601000                            | 23.9                                 |
| Sag 15            | 1981            | 2014 | 370 and 632    | 195 + 99.94         | 534000                            | 24                                   |
| Sag 20            | 1985            | 1998 | 408.2          | 81.8                | 155000                            | 24.6                                 |
| Sag 21            | 1989            | 2013 | 673.1          | 115.9               | 133000                            | 19.1                                 |
| <b>Matacães 2</b> |                 |      |                |                     |                                   |                                      |
| Sag 18            | 1986            | 2013 | 595            | 585                 | 1236000                           | 25.9                                 |
| Sag 19            | 1988            | 2006 | 723.5          | 255.5               | 604000                            | 27.4                                 |
| Sag 22            | 1990            | 2006 | 471 and 670    | 29 + 306            | 429000                            | 20.2                                 |
| Sag 24            | 2000            | 2013 | 1150           | 344                 | 441000                            | 20.2                                 |
| Sag 25            | 1991            | 2013 | 655 and 953    | 30 + 267            | 594000                            | 25.2                                 |
| Sag 26            | 1992            | 2013 | 522 and 590    | 68 + 552            | 876000                            | 21.2                                 |
| Sag 27            | 2001            | 2013 | 1200           | 292                 | 467000                            | 22.6                                 |

### c. Description of observed phenomenologies

The principal phenomena that affect the caverns in the short or long term are the following:

- brine warming: because the water injected into the caverns was generally colder than the surrounding salt, its contact with the salt bed generates thermal expansion of the brine (produced by salt dissolution during operations). This expansion induces, depending on whether the cavern is open or closed, brine discharge or an increase in cavern pressure, respectively;
- cavern convergence by salt creep: rock salt is a viscoplastic rock with a zero deviator stress threshold. Once brine pressure is less than ground pressure, the cavern closes by salt creep;
- brine permeation through the salt bed: although very low, the salt bed's permeability is not zero, which allows a very slow migration of brine toward the cavern's exterior. This permeation tends to work in opposition to the pressure increase related to salt creep and brine warming.

## 2. Available modeling data

### a. Cavern geometry

A localization of the wellheads as well as the precise spatial position (including deviations) of the wells' linear and the caverns' geometries, measured by sonar, are available. Missing data, in particular the extension and characteristic dimensions of the lower zones of the caverns, were estimated by analyzing operations data.

Estimation of the caverns' volume  $V$  was made from knowledge of the volume of dissolved salt (by estimating the amount of insoluble in the cavern bottom). This was estimated from the tonnage recovered and adding the volume of salt remaining in the cavern(s). Volumes are given in **Table 1**.

Secondly, we sought to distribute this volume in space using sonar measurements of the caverns (which enabled an estimation of the geometry of the upper part of the caverns, in particular the average diameter of the superior cavern) and the dimension in  $z$  of the roof and wall of the cavern(s).

### b. Determination of the caverns' compressibility

The quantity relating the cavern's pressure rise ( $\Delta P$ ) to volumetric variation ( $\Delta V$ ) is the cavern's apparent compressibility  $\beta V$  ( $\beta$  is the compressibility factor), expressed by the following equation:

$$\beta V = \frac{\Delta V}{\Delta P}$$

To estimate the volume  $V$ , different cases can be considered depending on whether the well serves 1 cavity or 2 superimposed cavities and whether these cavities are connected to each other or with other surrounding cavities. The apparent compressibility  $\beta V$  was evaluated for all caverns based on the analysis of periodic purges (**Table 2**).

### c. Material properties

For the sake of modeling, the geometry was simplified, the wells crossing from the surface: a marly-argillaceous layer (almost without salt); an intermediary layer in which the salt content varies from 10% to 80%; the salt layer (in which the salt content is greater than 80%). The properties of the intermediary layer assume a linear variation between those of the marly-argillaceous layer and the salt. The following properties were retained (see [2], [1], [6], [4], [5]) :

- marly-argillaceous and intermediary layers (an elastic behavior is assumed): Young's modulus = 15 GPa; Poisson ratio = 0.25; density = 2300 kg/m<sup>3</sup>; specific heat = 920 J/kg/K; thermal conductivity = 3.26 W/m/K ;
- salt (an elasto-viscoplastic behavior that can be described by combining a creep law associated to an elasto-plastic law with a Mohr-Coulomb-type failure criterion is assumed): Young's modulus = 25 GPa; Poisson ratio = 0.27; density = 2150 kg/m<sup>3</sup>; thermal expansion coefficient = 4.10<sup>-5</sup> 1/K; specific heat = 920 J/kg/K; thermal conductivity = 5.86 W/m/K;
- brine: density = 1200 kg/m<sup>3</sup>; thermal expansion coefficient = 4.4 10<sup>-4</sup> 1/K; specific heat = 3765 J/kg/K; equivalent thermal conductivity = 38400 W/m/K.

**Table 2.** Synthesis of the estimation of the apparent compressibility  $\beta V$  and the compressibility factor  $\beta$  from purge data

| Well number | $\beta V$<br>(m <sup>3</sup> / bar) | $\beta$<br>(10 <sup>-4</sup> MPa <sup>-1</sup> ) | Preliminary deduction from purge data                          |
|-------------|-------------------------------------|--|--|
| Sag 3       | 6,5                                 | 3,7  | Cav3 <sub>sup</sub> and Cav3 <sub>inf</sub> seem not connected |
| Sag 4       | 4,4                                 | 5,6  |  |
| Sag 5       | 40,6                                | <b>7,4</b>                                       | Cav5 <sub>sup</sub> and Cav7 seem connected                    |
| Sag 6       | 24,0                                | 4,8  | Cav6 and Cav7 could be connected                               |
| Sag 7       | 40,6                                | <b>7,4</b>                                       | Cav7 and Cav5 <sub>sup</sub> seem connected                    |
| Sag 8       | 15,1                                | 5,4  |  |
| Sag 9       | 19,1                                | 4,5  |  |
| Sag 10      | 21,0                                | 4,4  |  |
| Sag 12      | 10,2                                | <b>5,5</b>                                       | Cav12 <sub>sup</sub> and Cav12 <sub>inf</sub> are connected    |
| Sag 13      | 34,4                                | 4,2  |  |
| Sag 14      | 26,6                                | 4,4  |  |
| Sag 20      | 9,6                                 | <b>6,2</b>                                       |  |
| Sag 21      | 6,5                                 | 4,9  |  |
| Sag 18      | 56,7                                | 4,6  |  |
| Sag 19      | 25,7                                | 4,3  |  |
| Sag 22      | 18,8                                | 4,4  | Cav22 <sub>sup</sub> and Cav22 <sub>inf</sub> are connected    |
| Sag 24      | 16,7                                | 3,8  |  |
| Sag 25      | 22,0                                | 3,7  | Cav25 <sub>sup</sub> and Cav25 <sub>inf</sub> are connected    |
| Sag 26      | 36,4                                | 4,2  | Cav26 <sub>sup</sub> and Cav26 <sub>inf</sub> are connected    |
| Sag 27      | 18,3                                | 3,9  |  |

Additional properties were considered for salt:

- Creep parameters: salt creep was modeled according to the 3-parameter Norton-Hoff law:  $m$  [-];  $Q/R$  [K];  $A$  [year<sup>-1</sup>]. The value of "m" was estimated to be 2.47 in a previous study based on experimental results [4]. The "best" parameters were obtained by calibration from measurements of the evolution of the brine pressure in the wellhead between two purges and the brine discharge from an open well during creep tests;
- Properties defining the failure criterion: laboratory tests [4] led to a proposed tensile strength value of  $R_t = 1.3$  MPa and an expansion phase threshold of 25 MPa (deviator stress value). We also proposed to examine the risk of shear failure based on a Mohr-Coulomb criterion defined by a cohesion of 2 MPa and an angle of internal friction of 20° (very conservative values);
- Intrinsic permeability of salt [m<sup>2</sup>]: the chosen value for the benchmark model is 10<sup>-19</sup> m<sup>2</sup>. We shall see below the strong dependence of long-term equilibrium pressure to this choice.

#### d. Temperature profile

Temperature profiles were developed for the caverns. They serve to indicate the current temperatures in the caverns as well as the thermal gradients in the recovery (which will allow specification of the thermal boundary conditions to be applied laterally, **Figure 1**).

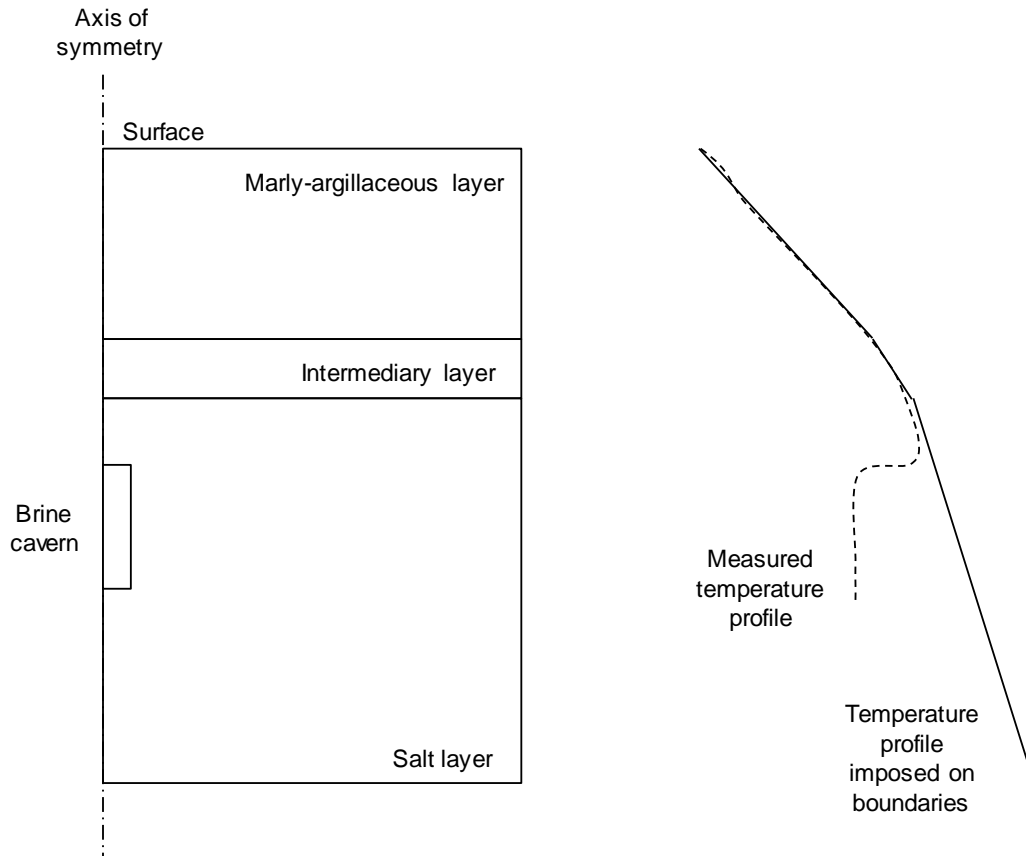


**Figure 1.** Thermal boundary conditions

The sensor measures brine temperature at different depths in the well or cavern. Brine temperature in the well is expected to be in equilibrium with that of the surrounding rock. Yet, it is necessary to purge the cavern before measuring, which brings up the brine present in the depths (thus having a higher temperature than that initially in place) toward the surface. We have shown that is better to wait approximately 24 hours after purging to carry out the profile so that the temperature of the brine in the well can return to equilibrium with that of the bed.

**Figure 2** shows two profiles that illustrate a thermal gradient of  $0.04^{\circ}\text{C}/\text{m}$  in the marl and  $0.0226^{\circ}\text{C}/\text{m}$  in the salt. We were able to confirm that these gradients were consistent with a thermal conductivity of  $3.26\text{ W}/\text{m}/^{\circ}\text{C}$  for marl and  $5.86\text{ W}/\text{m}/^{\circ}\text{C}$  for salt. Moreover, the brine's convective mixing tends to equalize brine temperature in the cavern ( $30.5^{\circ}\text{C}$  in cavern 6 and  $46^{\circ}\text{C}$  in cavern 27).

Still, the temperature profiles are not all consistent (temperature variation close to the surface, variation of thermal gradients in the marl or salt). This can be explained either by a heterogeneity of the geological formations of the different wells or the diapir's overall cooling linked to the massive injection of fresh water (the injection temperature is approximately  $16^{\circ}\text{C}$  on average) over several dozen years. The fact that the observed anomalies concern primarily Matacães 1 supports this assumption.

We noted that thermal boundary conditions based on a poor evaluation of thermal gradients (overestimated for Matacães 1 with the selection of  $0.04^{\circ}\text{C}/\text{m}$  in marl and  $0.0226^{\circ}\text{C}/\text{m}$  in salt) artificially increases the difference between the brine temperature in the cavern (correctly estimated) and the temperature in the surrounding salt (poorly estimated). This initial error led to an overestimation of the impact of the brine's warming to such an extent that the model predicts pressure increases or brine discharges linked to thermal expansion greater than measured values, before also taking into account the creep effect. Calibration of the temperature profiles led to modification of the gradient values.

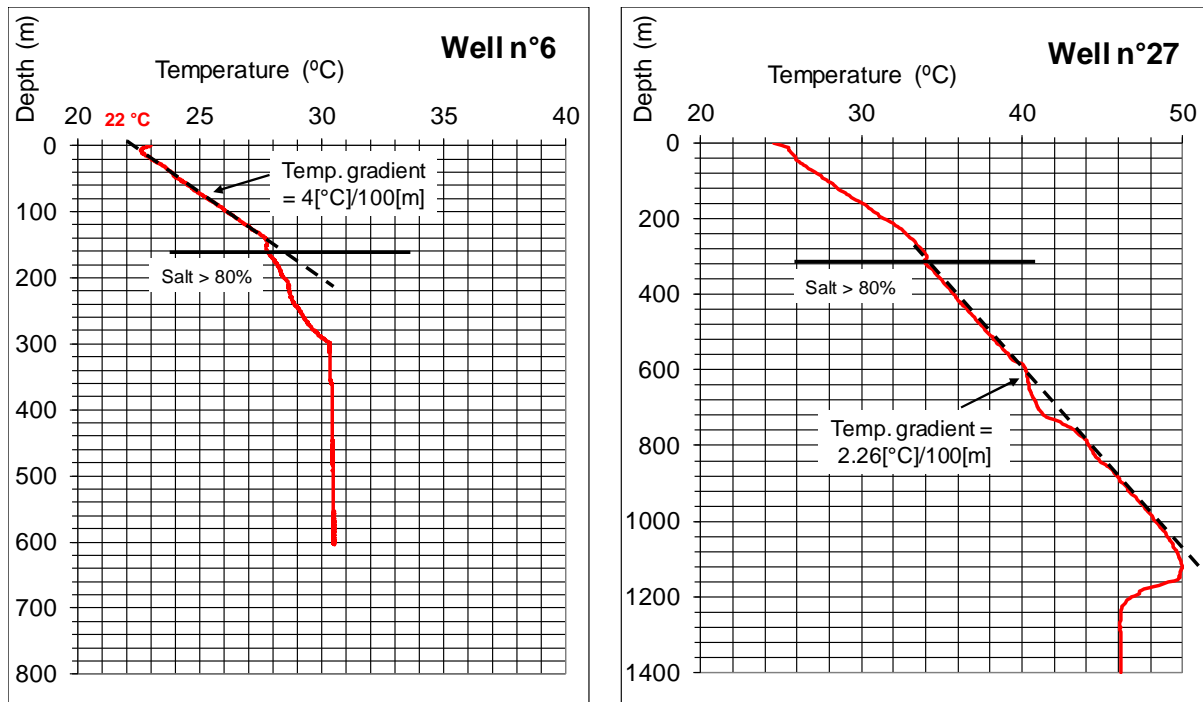


**Figure 2.** Temperature profile for wells Sag 6 and Sag 27

Caverns 3, 4, 5, 6, 7, 9, 10 and 20 are seemingly at thermal equilibrium. As indicated in **Table 1**, these caverns have a volume between 79,000 m<sup>3</sup> (cavern 4) and 500,000 m<sup>3</sup> (cavern 6) and have not been operated since between 1974 (cavern 5) and 2002 (cavern 10).

Caverns 12, 13, 14, 15, 18, 19, 21, 25, 26 and 27 are not yet at thermal equilibrium (**Table 3**). As indicated in **Table 1**, these caverns have a volume between 133,000 m<sup>3</sup> (cavern 21) and 1,236,000 m<sup>3</sup> (cavern 18) and have not been operated since between 2006 (cavern 19) and 2014 (caverns 13, 14 and 15). An increase in brine temperature in these caverns is observed, corresponding to a progressive warming induced by the surrounding salt (because the temperature sensor was replaced in 2016, the measured variations for caverns 14, 19 and 25 could be inaccurate).

**Table 3.** Synthesis of the wells' temperature profiles

| Well number | Brine temperatures in the cavern<br>(*: the measurement was taken in 2015 with a different sensor) |                       | ΔT       | Average temp. at surface |
|-------------|--|-----------------------|----------|--------------------------|
|             |  |                       |          |                          |
| 12          | 29.26°C (20/10/2016)   | 29.39°C (20/11/2017)  | +0.13°C  | 21°C                     |
| 13          | 31.40°C (2/11/2016)  | 31.79°C (25/10/2017)  | +0.39°C  | 21°C                     |
| 14          | 31.70°C (16/11/2015)*  | 32.08°C (21/10/2016)  | +0.38°C? | 20°C                     |
| 15          | 26.29°C (24/10/2016)   | 26.67°C (27/7/2017)   | +0.38°C  | 16°C                     |
| 18          | 35.24°C (13/10/2016)   | 35.75°C (30/10/2017)  | +0.51°C  | 24°C                     |
| 19          | 37.4°C (3/11/2015)*  | 37.85°C (27/10/2017)  | +0.45°C? | 22°C                     |
| 20          | 30.98°C (31/10/2016)   | 31.03°C (9/11/2017)   | +0.05°C  | 20°C                     |
| 21          | 37.51°C (13/10/2016)   | 37.86°C (30/10/2017)  | +0.35°C  | 19°C                     |
| 25          | 31.24°C (18/11/2015)*  | 33.84°C (13/10/2017)  | +2.6°C ? | 23°C                     |
| 26          | 27.21 °C (10/8/2016)   | 28.35 °C (3/11/2017)  | +1.14°C  | 22°C                     |
| 27          | 47.06 °C (3/11/2016)   | 47.92 °C (10/11/2017) | +0.86°C  | 24.5°C                   |

### 3. Calibration of creep parameters

The objective is to determine the creep parameters from, respectively, the measurement of the brine pressure rise in the wellhead between 2 purges and the measurement of the average brine discharge during creep tests. To this end, a “global” model taking into account the phenomenologies described above and adapted to the simulation of these two measurements was developed. Given the duration of the tests, the phenomenologies at the origin of the measured variations are primarily the brine’s thermal expansion and salt creep. Permeation had only a very slight impact on the results (verified for cavern 6 assuming a permeability variation of  $10^{-18}$  m<sup>2</sup> to  $10^{-20}$  m<sup>2</sup>). Under the condition that the thermal effects have been correctly estimated (or are negligible), calibrating models on pressure variations or measured discharge should enable alignment of the creep parameters.

#### a. "Global" model developed to calculate brine temperature evolution and average pressure in the cavern

We present here the “global” model (non-spatialized) developed to calculate the evolution of brine pressure in the cavern. It is a semi-analytical model based on the Bérest and Brouard formulas [1], taking into account simultaneously (or not) the effects of the brine’s thermal expansion, salt creep and the permeation of brine into the salt. These formulas were imported and resolved with Comsol Multiphysics modeling software [8]. The model depends on the following assumptions:

- the cavern is assimilated to a cylinder (of radius  $R_c$  and height  $H_c$ ) of which the center is located at a depth  $h$ ;
- the cavern is completely filled with brine;
- it is surrounded by a salt bed assumed to be homogenous and isotropic. The salt’s behavior is assumed to be described by the Norton-Hoff law, which, for an underground, cavern-type structure, links the salt’s deformation velocity to brine pressure in the cavern. These relations involve the 3 following parameters: deviator stress exponent  $m$  [unitless], activation energy ratio over the Boltzmann constant  $Q/R$  [K], and reference  $A$  [year<sup>-1</sup>] velocity;
- the cavern’s evolution over time is described by the following global variables: average brine temperature in the cavern ( $T_s$ ), average brine pressure in the cavern ( $P_s$ ), cavern volume ( $V$ );
- the thermo-hydro-mechanical properties of salt and brine are assumed to be constant both spatially and over time for a given simulation mode.

Furthermore, we assume an initially isotropic and lithostatic stress state within the salt bed and an initially linear variation of temperature with depth.

The initial values of the model’s variables are the following:  $T_s^{(t=0)}$ : in most cases, it will be equal to the measured value;  $P_s^{(t=0)}$ : in most cases, it will be equal to halmostatic pressure (pressure exerted by a brine column rising to the surface);  $V^{(t=0)}$ : value of the considered cavern’s volume.

#### b. Implemented methodology

We proceeded in the following manner:

- for each well, a post-purge pressure rise (start date, end date, measured overpressure) and the measured brine discharge during creep test (start date, end date, average measured discharge) were identified;
- for each well, the temperature profile done immediately prior to the start date of the chosen pressure rise or creep test was chosen;
- phase 1: the thermal model (surface temperature, value of thermal gradients in the marl and salt) was calibrated so as to best reproduce the last measured temperature profile;
- phase 2: the thermal state at the beginning of the pressure rise or considered creep test was estimated by means of this model;
- phase 3: a series of simulations for each well was performed to reproduce the pressure rise or creep test discharges by using the global model. We varied the 3 creep parameters in the following value ranges:  $2.4 < m < 2.6$ ;  $3400 \text{ K} < Q/R < 4400 \text{ K}$ ;  $4 \text{ [year}^{-1}\text{]} < A < 6 \text{ [year}^{-1}\text{]}$ . The objective is to determine for each well the parameters that renders the measured values (overpressure or average discharge). It should be noted that salt creep increases when “ $m$ ” and “ $A$ ” increase and when  $Q/R$  decreases.

The phenomena taken into account during phase 3 are brine expansion and creep. This is totally justified in the case of creep tests because permeation is zero when brine is at halmostatic pressure. In the

case of the simulation of pressure increases, we verified that given the test duration, discharge variations linked to permeation are negligible, even assuming a low salt permeability. Given the uncertainties concerning the evaluation of thermal effects (related in particular to the difficulty in assessing the thermal gradient in the salt layer), particularly for Matacães 1, we preferred to only take into account effects related to salt creep in the case of caverns assumed to be at thermal equilibrium (served by wells 3, 4, 5, 6, 7, 9, 10, 20). All the same, it should be noted that the dependence of creep on temperature is always taken into account.

### c. Application to the simulation of the brine pressure rise between 2 purges

As an illustration, we present work carried out for cavern 27. For this cavern, we selected the following data:

- Start date of the pressure rise: 9/2/2017
- End date of the pressure rise: 3/3/2017
- Pressure rise measured between these 2 dates: 8.1 bars
- Duration of the pressure rise: 22 days

The evolution of pressure in the wellhead is represented in **Figure 3**. Thermal profiling was done in this well the 3/11/2016, 98 days before. The brine temperature in the cavern on this date was 47.16°C.

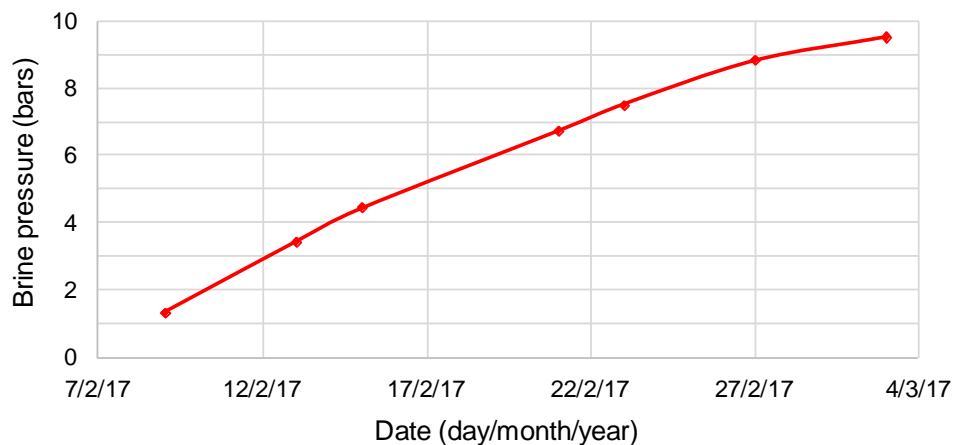


**Figure 3.** Evolution of pressure measured in the wellhead between 9/2/2017 and 3/3/2017 for Sag 27

The calibration results are presented in **Figure 4**. The best triplet in this case is:  $m = 2.4$ ;  $Q/R = 4000$  K;  $A = 4$  [year<sup>-1</sup>]. It should be noted that the pressure increase is primarily due to salt creep. Indeed, calculations show that the increase related to the brine's thermal expansion (due to a warming of 0.03°C during the 22 days of the rise) is only 4.2% of the total (or 0.34 bars of the 8.1 bars).

The results obtained for the entirety of the caverns lead to the following observations:

- the triplets determined for wells 3, 4, 5, 6, 7, 9 and 12 are relatively close (**Figure 5**) in accordance with the caverns' proximity to each other (Q/R values varying from 3600 to 3700);
- wells 8 and 10, slightly set off to the east, have a bit higher Q/R (4000 instead of 3600). Wells 13 and 14, even more set off toward the east, have a Q/R of 4200. Well 21, at the extreme east, has a Q/R of 4400. Yet, a Q/R of 3800 was obtained for well 20, situated next to it;
- with the exception of wells 22 and 25 (Q/R of 4200 and 4300 respectively), the Matacães 2 wells (18, 19, 24, 26 and 27) have a Q/R of approximately 4000.

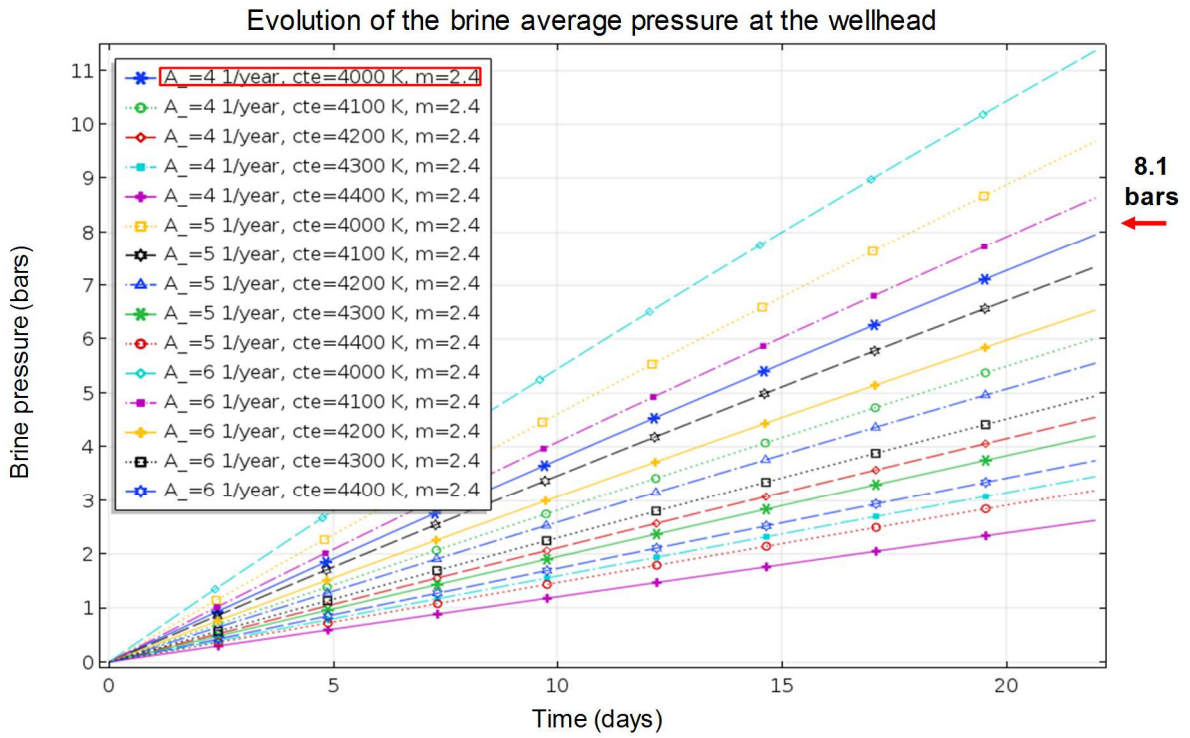


**Figure 4.** Simulation of the increase in brine pressure in the wellhead between 9/2/2017 and 3/3/2017 for Sag 27 (other simulations were done with  $m=2.5$  and  $2.6$ )

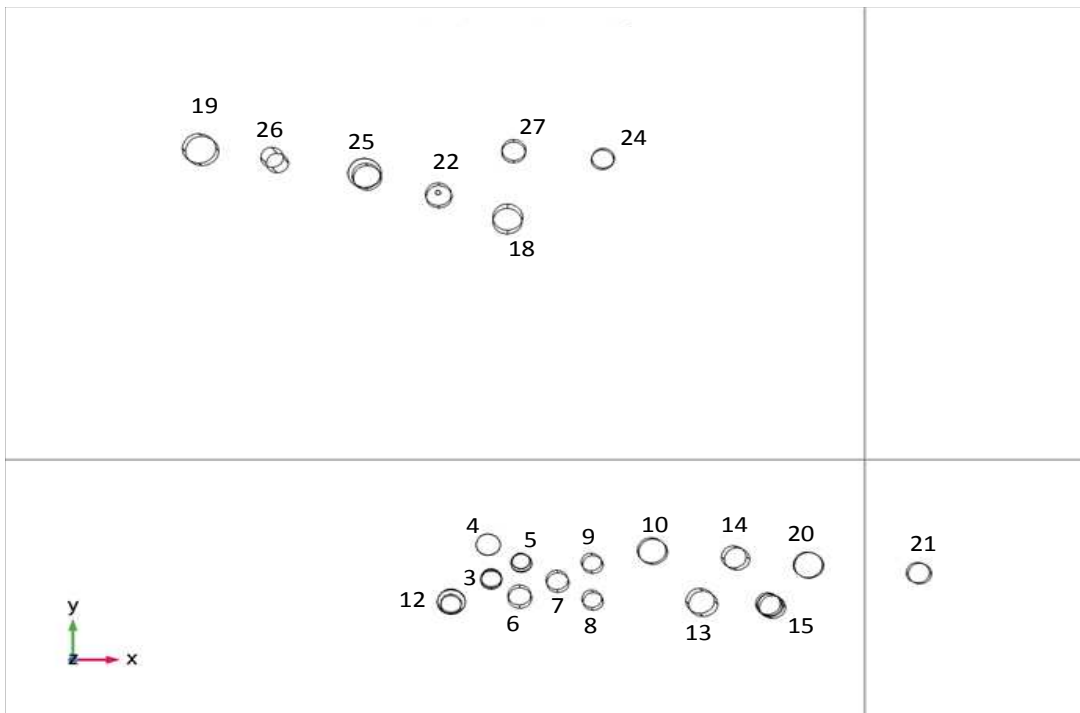


**Figure 5.** Plan view showing wellhead locations

#### d. Application to the simulation of creep tests

As an illustration, we present the work carried out for cavern 27. The data from the creep test for this cavern are the following:

- Start date of the test: 14/11/2016
- End date of the test: 22/11/2016
- Test duration: 8 days
- Average measured discharge: 460 liters/h = 7.7 liters/mn

The evolution of the well discharge is represented in **Figure 6**. Thermal profiling was done in this well 3/11/2016, 11 days earlier.

The calibration results are presented in **Figure 7**. The best triplet in this case is:  $m = 2.6$ ;  $Q/R = 4000$  K;  $A = 5$  [year<sup>-1</sup>]. This triplet is again close to the one determined from the post-purge pressure rise measurement for the same well ( $n = 2.4$ ;  $Q/R = 4000$  K;  $A = 4$  [year<sup>-1</sup>]). We calculated that the share of the discharge related to brine expansion in this case was 2% (or 0.16 liters/mn). It is considered to be negligible and corresponds to the brine's warming by 0.01°C during the 8 days of the test.

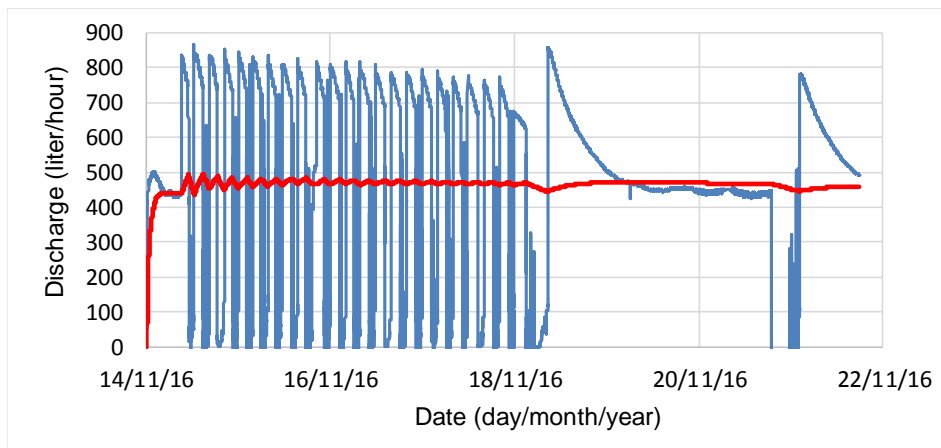


**Figure 6.** Evolution of the discharge measured in the wellhead for Sag27 between 14/11/16 and 22/11/16 (blue: instantaneous value; red: average value)

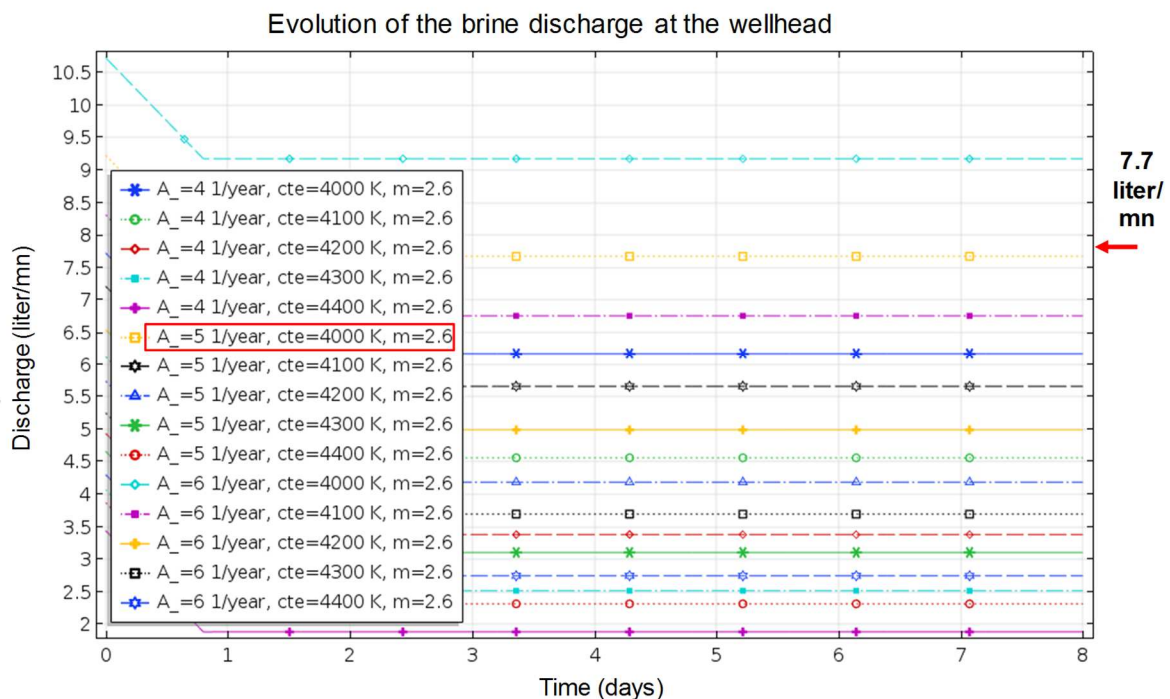


**Figure 7.** Simulation of the brine discharge from the wellhead between 14/11/2016 and 22/11/2016 for Sag 27 (other simulations were done with  $m=2.4$  and  $2.5$ )

The results obtained for the entirety of the caverns lead to the following observations:

- the triplets determined for wells 3, 4, 6, 9 and 12 are again relatively close with Q/R values varying from 3400 to 3700 (values of the same order but a little more dispersed than those obtained from the pressure increases);
- wells 10, 13 and 14, slightly set off toward the east, have a slightly higher Q/R (from 4000 to 4100). The Q/R obtained for well 21 at the extreme east is again high (4400), while that of well 20 is again relatively low (3600);
- wells 22 and 25 have a Q/R of 4200 and 4100 respectively, while the other Matacães 2 wells (19, 24, 26 and 27) have a Q/R of approximately 4000.

#### e. Conclusion

This calibration method favors a correct reproduction of the measurements for each cavern for the determination of the intrinsic rheological parameters of Matacães salt. The results demonstrate some variability in the creep parameters. We believe the logical explanation of this variability can be found in the salt diapir's relative heterogeneity at the considered scale. The low dispersion of the parameters for the closest caverns tends to confirm this hypothesis. Furthermore, one notes (overall) that the results obtained from pressure measurements and those from discharge measurements are consistent.

### 4. Development of a 2D-axi predictive model

#### a. Description of the model

This is a spatialized thermo-mechanical model combining temporal (time steps) and spatial (mesh) discretization. The model can be described as follows:

- the conductive heat exchanges in the brine (equivalent conductivity), salt and recovery are modeled;
- the mechanical behavior of the salt and recovery are also simulated. The mechanical effect of brine pressure on the cavern's walls is imposed as a boundary condition, the brine pressure's evolution being calculated in parallel by means of the global model described above;
- it is a coupled thermo-mechanical calculation that takes into account at each time step the stress variations induced by the variation of the salt and recovery's temperature fields.

The model has 2 temporal phases:

- Phase 1: calculation of the cavern's behavior in an "open-well" configuration from the fixed initial time (the date of the last temperature profile, for example). The duration of this phase is the time until definitive plugging. In the examples below, we set the duration of this phase at only one year, which is very short, as we will see, for offsetting thermal effects. During this phase, brine pressure remains constantly equal to halmostatic pressure. Pressure fluctuations related to the alternance of temporary plugging and purges were ignored (insofar as they remain less than 1 MPa). The model calculates the decrease in the cavern's volume and brine discharge from the well due to brine warming and salt creep. We chose to use the creep parameters obtained from creep tests insofar as the model used for the calibration depends on similar hypotheses as those considered during phase 1;
- Phase 2: calculation of the caverns' behavior after definitive plugging. This phase's duration is 500 years after definitive closure. During this phase, the model calculates the evolution of brine pressure related to the combined effects of salt creep, the brine's thermal expansion and its permeation into the salt bed. We chose to use the creep parameters obtained from the pressure rise measurements insofar as the model used for the calibration depends on similar hypotheses as those considered during phase 2.

It was applied to all of the wells (one model per well). Adjustments were necessary depending on whether the well served 1 cavern or 2 superimposed caverns, they were hydraulically connected, or one of the caverns was connected to a surrounding cavern. A classification was made from the purge analysis (calculation of the compressibility factor; compared pressure evolutions). In-progress sealing tests will also enable validation and clarification of this classification.

Furthermore, in the 2D-axi models, for caverns assumed to be at thermal equilibrium, we chose to only take into account the effects related to salt creep. Concretely, that consisted of deactivating the effects related to the brine and salt's thermal expansion. In all cases, the dependence of brine on temperature is conserved.

**b. Presentation of the results for cavern 27**

The evolution of brine temperature is represented in **Figure 8**. Its temperature increases by 10°C in 500 years, with an equilibrium temperature of approximately 57°C. Warming is initially more rapid, the temperature of 56°C being reached after 88.5 years. One notes that the temperature is homogenized in the cavern through convective mixing.

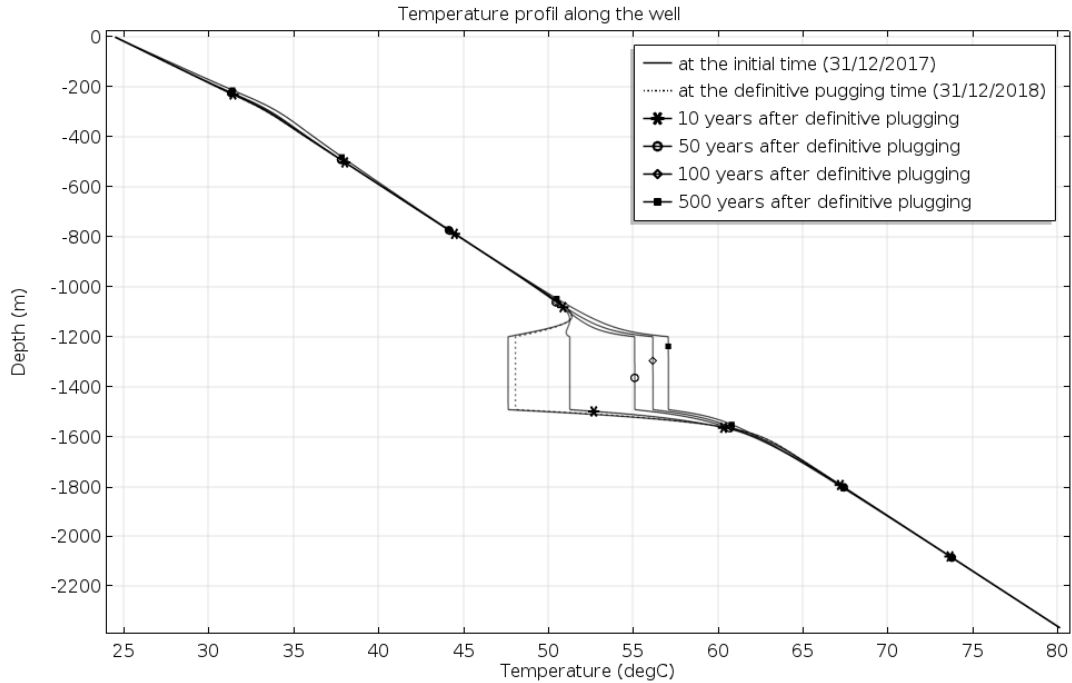


**Figure 8.** Temperature profile evolution along well “Sag 27”

**Figure 9** shows the evolution over time of brine pressure in the center of the cavern. It is equal to halmostatic pressure during the “open-well” phase 1. After definitive plugging of the well (31/12/2018 in the benchmark model), brine pressure rapidly increases to reach the maximum value of 27.25 MPa approximately 14 years later. It then decreases to reach an equilibrium pressure slightly less than approximately 26.5 MPa. The peak is related to the thermal effect, which has the fastest kinetics. Equilibrium pressure is only related to the combined effects of creep and permeation.

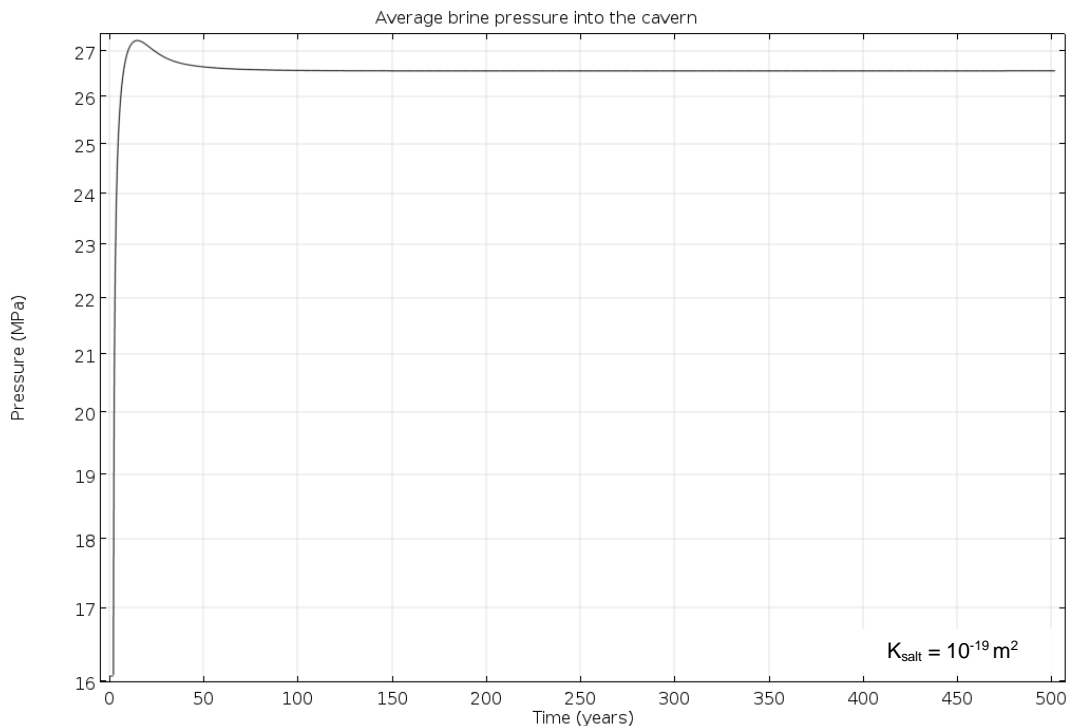


**Figure 9.** Evolution of average brine pressure in cavern 27

**Figure 10** examines tensile failure risks when brine pressure in the cavern exceeds the value of lithostatic stress within the salt.

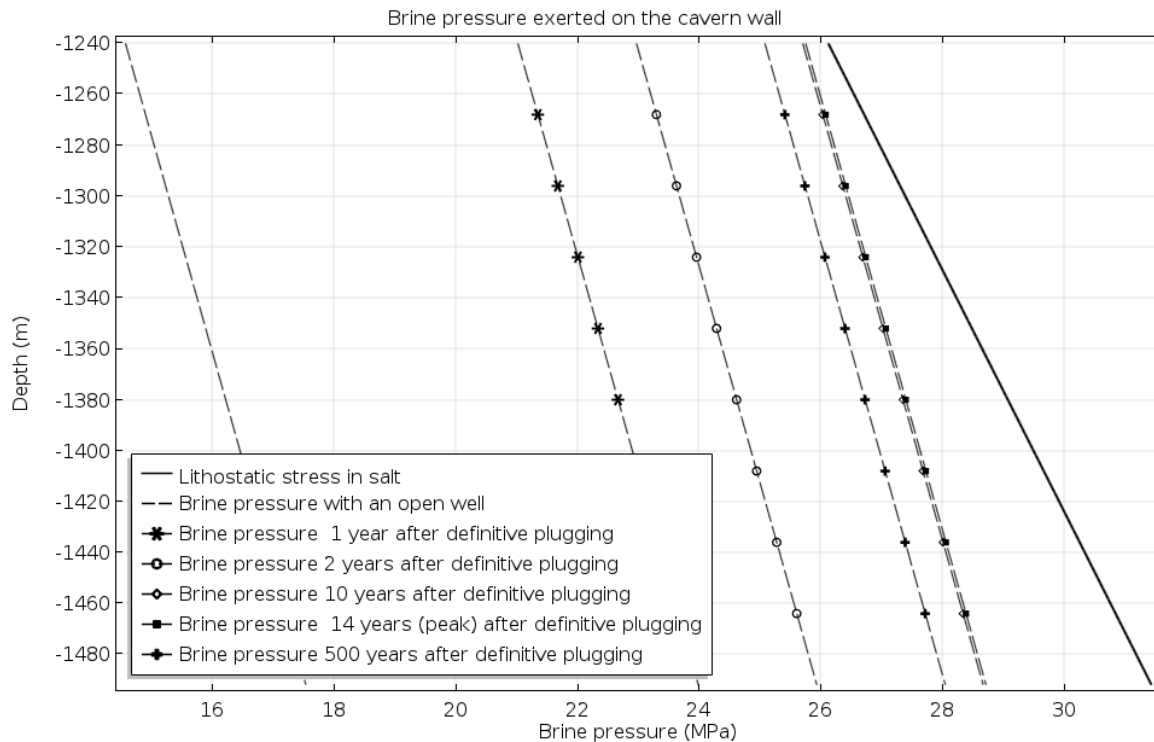


**Figure 10.** Evolution of brine pressure exerted on the walls of cavern 27 compared to lithostatic stress within the salt (2D-axi model)

For each profile, the evolutions between the roof (-1240 m) and the wall (-1492 m) are related to the densities of brine ( $d_{\text{brine}}=1.2$ ) and salt ( $d_{\text{salt}}=2.2$ ). The brine profiles get progressively closer to the lithostatic stress profile, reaching their closest at the time of the thermal peak (14 years after definitive closure), and then grow farther apart. Thus, for the benchmark case, one notes that tensile failure risk seems precluded (with some uncertainty, all the same, given the proximity of the brine pressure profile at 14 years with the lithostatic stress pressure profile).

**Figure 11** now shows the evolution of the cavern’s volume over time after definitive plugging of the well. According to the global model, the volume decreases by approximately 5.7% after 500 years. This is consistent with the displacements calculated with the 2D-axi model by which one determines a maximum wall displacement of 1.83 m, the highest values being obtained at the cavern’s base (zones in which displacement is less than 0.05 m are masked).

The evolution of the Von Mises stress is indicated in **Figure 12**. The Von Mises stress is equal to  $(3J_2)^{0.5}$ , where  $J_2$  is the second invariant of the stress deviator tensor  $\sigma_d = \sigma + p I$ , where  $\sigma$  is the stress tensor and  $p = 1/3 \text{ trace}(\sigma)$ . The zones in which this stress is greater than 9 MPa and less than 25 MPa (expansion phase threshold retained for Matacães salt by [4][3]) were visualized. The much lower 9 MPa threshold is sometimes proposed in the literature [5]. The zones with values greater than or equal to 25 MPa (zones in red) are relatively small and located in the cavern’s angular areas. The zones with values greater than 9 MPa form a thin layer around the cavern. After closure, pressure in the cavern increases and reduces deviator stresses within the walls, which explains the disappearance of this layer after 100 years. We also identified the shearing failure zones in which the defined plasticity criterion is reached (see section 2.c.). They are observed very locally in the cavern’s angular areas.

### c. Impact of salt permeability – the case of cavern 27

The intrinsic permeability of in situ salt is not precisely known. In general, its value is estimated as varying between  $10^{-20} \text{ m}^2$  and  $10^{-18} \text{ m}^2$ . The value of equilibrium pressure is dependent on permeability. The more impermeable the salt, the closer equilibrium pressure will be to the lithostatic stress value.

Inversely, the greater the salt permeability, the closer equilibrium pressure will be to halmostatic pressure. The abandonment tests necessary for some caverns should help determine equilibrium pressure in each cavern and deduce the value of salt permeability.

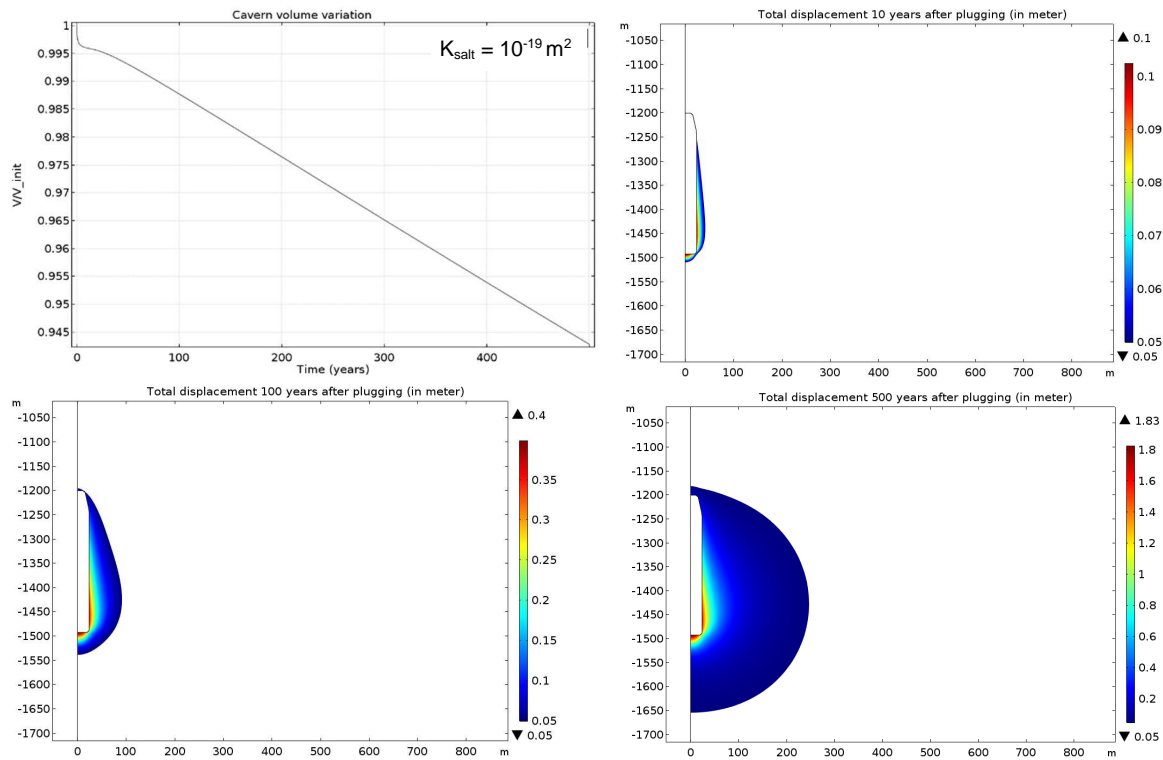


**Figure 11.** Decrease in the volume of cavern 27 due to salt creep (at left: the “vol. / init. vol.” ratio calculated by the global model; at right: total displacements calculated by the 2D-axi model after plugging: after 10 years (max: 0.1 m wall), 100 years (max: 0.4 m) and 500 years (max: 1.8 m).

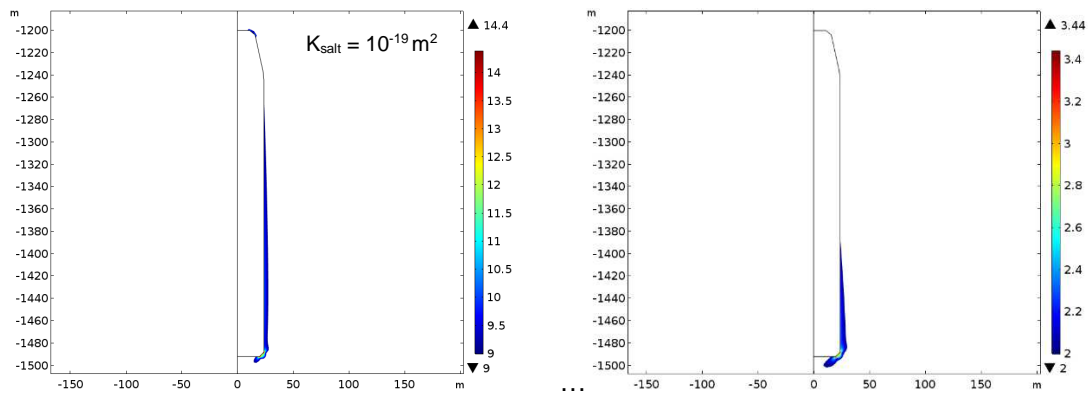


**Figure 12.** Von Mises isostress values (in MPa) around cavern 27 today (max: 14.4 MPa) and 100 years after definitive closure (max: 3.44 MPa). The zones with values less than 9 MPa (today) or 2 MPa (100 years after definitive closure) are masked.

In the case of cavern 27, we performed a sensitivity study for the following 3 values:  $10^{-20} m^2$ ,  $10^{-19} m^2$  (benchmark case) and  $10^{-18} m^2$ . For this study, the waiting time (duration of the “open-well” phase) was set at 1 year. Since thermal evolutions are not dependent on salt permeability, they are the same for all 3 values. Mechanical evolutions during the waiting phase are also unaffected by salt permeability, as during this phase brine pressure remains constantly equal to halmostatic pressure.

After plugging, however, one observes a modification in the evolution of brine pressure and the cavern’s volume (Figure 13).

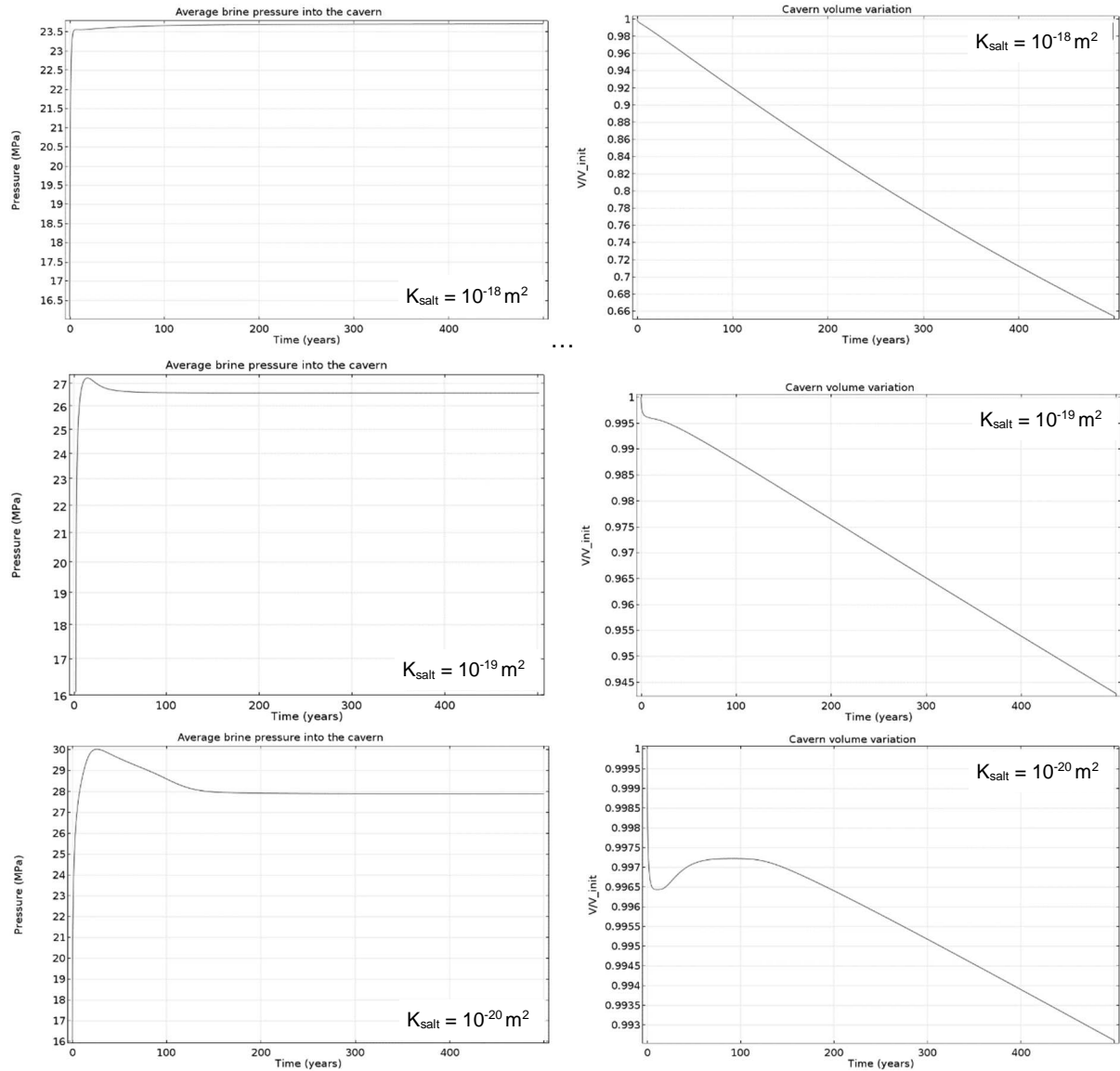


**Figure 13.** Evolution of the average brine pressure in cavern 27 and its volume depending on the selected salt permeability - Max. pressure: 23.7 MPa ( $10^{-18} \text{ m}^2$ ), 27.3 MPa ( $10^{-19} \text{ m}^2$ ) and 30.0 MPa ( $10^{-20} \text{ m}^2$ ) – Loss of vol. after 500 years: 34% ( $10^{-18} \text{ m}^2$ ), 5.7% ( $10^{-19} \text{ m}^2$ ); 0.7% ( $10^{-20} \text{ m}^2$ ).

The increase in salt permeability from  $10^{-19} \text{ m}^2$  to  $10^{-18} \text{ m}^2$  allows the overpressures induced by brine expansion and salt creep to dissipate more rapidly, to such an extent that the pressure peak disappears. To the contrary, when permeability decreases from  $10^{-19} \text{ m}^2$  to  $10^{-20} \text{ m}^2$ , the pressure peak becomes more significant (from 27.3 to 30.0 MPa) and lasts longer (from 40 to 120 years).

The high calculated brine pressure values in the case of low permeability act in opposition to the cavern's creep due to the reduced deviator stress within the walls. This explains why the volume loss 500 years after definitive closure decreases from 34% to 0.7% when permeability decreases from  $10^{-18} \text{ m}^2$  to  $10^{-20} \text{ m}^2$ . An inverse creep even appears between 10 and 100 years after definitive plugging in the case of a permeability of  $10^{-20} \text{ m}^2$ . The total displacements are also highly affected by this permeability variation. Indeed, 500 years after definitive closure, maximum displacement decreases from 7.2 m (for  $10^{-18} \text{ m}^2$ ) to 0.6 m (for  $10^{-20} \text{ m}^2$ ).

The brine pressure exerting on the cavern wall becomes greater than the lithostatic stress in the salt for a salt permeability of  $10^{-20} \text{ m}^2$  (Figure 14). Thus, in this case, there would be a tensile failure risk for the salt. However, the deviator stresses increase with salt permeability due to decreased brine pressure. In this case, the shearing failure risk is greater, particularly in the cavern's base.

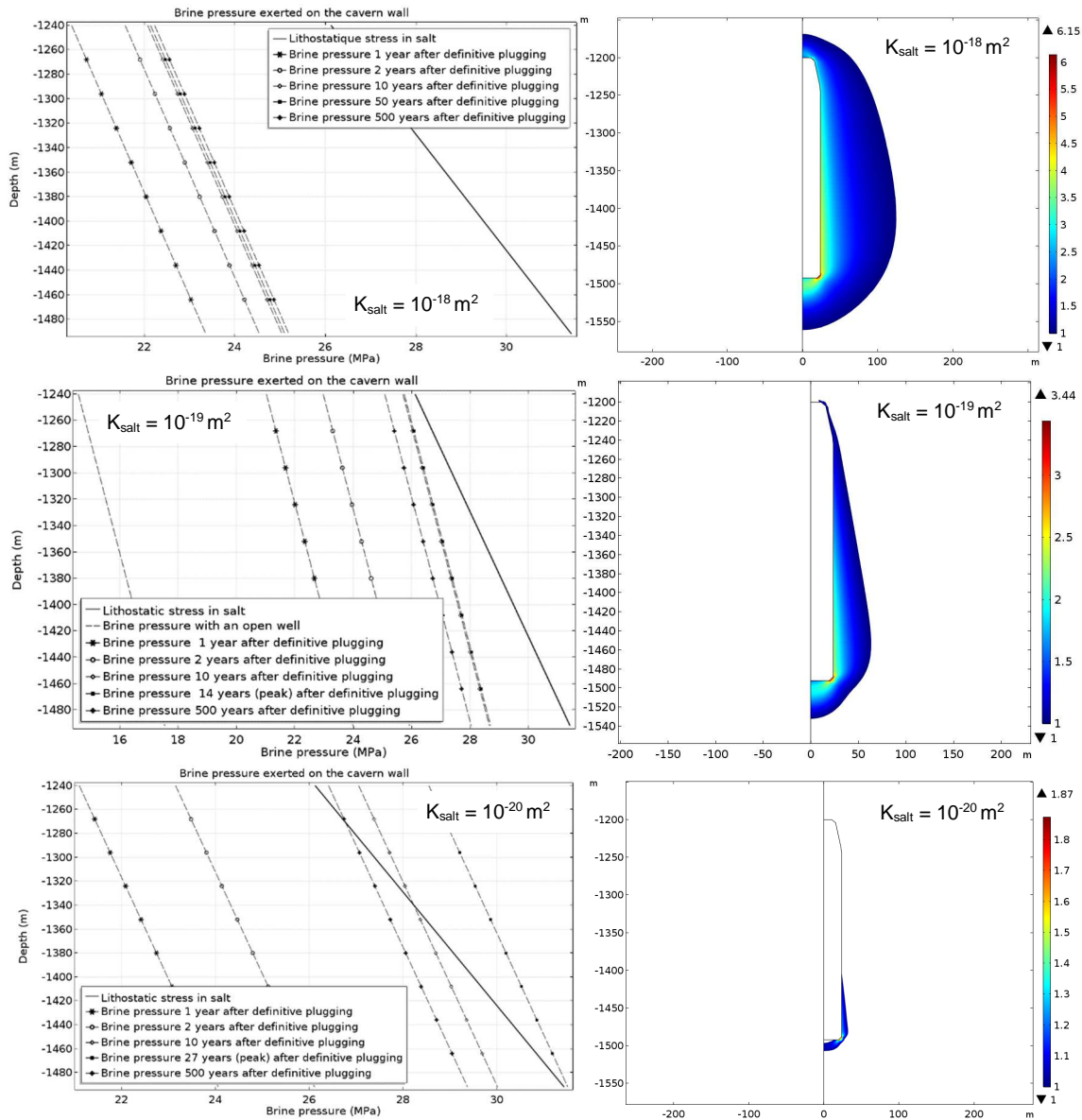


**Figure 14.** Impact of salt permeability: at left, on the evolution of brine pressure exerted on the cavern walls compared to the lithostatic stress within the salt; at right, on Von Mises iso-stress values calculated around the cavern (values in MPa) 100 years after definitive closure of the well. The zones in which the value is less than 1 MPa are masked

#### d. Impact of waiting time – the case of cavern 26

We saw above that the brine pressure peak was related to brine expansion after warming. One way to prevent the pressure peak from being too significant is to allow the brine to warm before definitive closure of the well. This amounts to increasing the waiting time  $t_w$  before plugging.

We studied the impact of this waiting time in the case of cavern 26, assuming 4 waiting times:  $t_w = 1$  year, 10 years, 20 years and 50 years. The salt permeability value was set at the benchmark value ( $10^{-19} \text{ m}^2$ ) in all cases.

**Figure 15** shows the evolution of average brine temperature in cavern 26 depending on waiting time before definitive plugging. Brine temperature at the time of closure increases in the following manner: 28.8°C ( $t_w = 1$  year); 33.0°C ( $t_w = 10$  years); 35.8°C ( $t_w = 20$  years); 39.4°C ( $t_w = 50$  years).

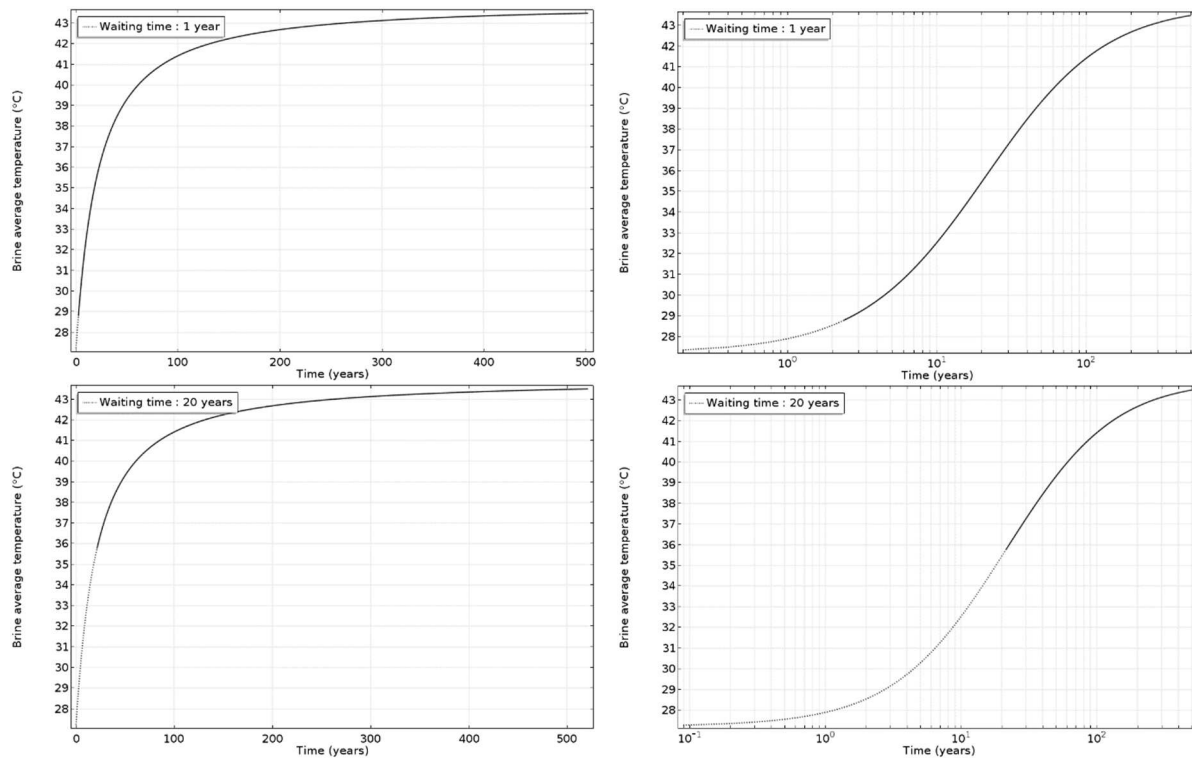


**Figure 15.** Evolution of average brine temperature in cavern 26 depending on the waiting time before definitive closure (“open-well” phase: dotted line; “after-plugging” phase: continuous line)

Reducing thermal disequilibrium before plugging has the effect of reducing maximum pressure: 17.35 MPa ( $t_w = 1$  year); 16.42 MPa ( $t_w = 10$  years); 16.09 MPa ( $t_w = 20$  years); 15.82 MPa ( $t_w = 50$  years). This decreased pressure leads to a reduction in the size of the tensile failure zone (**Figure 16**), which stretches from the cavern’s roof (-522 m) to (pressure peak value): -811 m ( $t_w = 1$  year); -712 m ( $t_w = 10$  years); -677 m ( $t_w = 20$  years); -649 m ( $t_w = 50$  years).

The impact of waiting time on the evolution of the cavern’s volume loss was calculated. At the time of plugging, this loss is the following: 0.4% ( $t_w = 1$  year); 2.1% ( $t_w = 10$  years); 4.3% ( $t_w = 20$  years); 11.4% ( $t_w = 50$  years). Logically, it increases with waiting time. After definitive plugging, the volume loss continues to reach 500 years after: 4% ( $t_w = 1$  year); 5.9% ( $t_w = 10$  years); 8.2% ( $t_w = 20$  years); 15.5% ( $t_w = 50$  years). The share after plugging is thus: 3.6% ( $t_w = 1$  year); 3.8% ( $t_w = 10$  years); 3.9% ( $t_w = 20$  years); 4.1% ( $t_w = 50$  years): it is little affected by waiting time. This is confirmed if one considers the total calculated displacements after plugging. Indeed, the maximum displacement is: 4.13 m ( $t_w = 1$  year); 4.22 m ( $t_w = 10$  years); 4.27 m ( $t_w = 20$  years); 4.34 m ( $t_w = 50$  years).

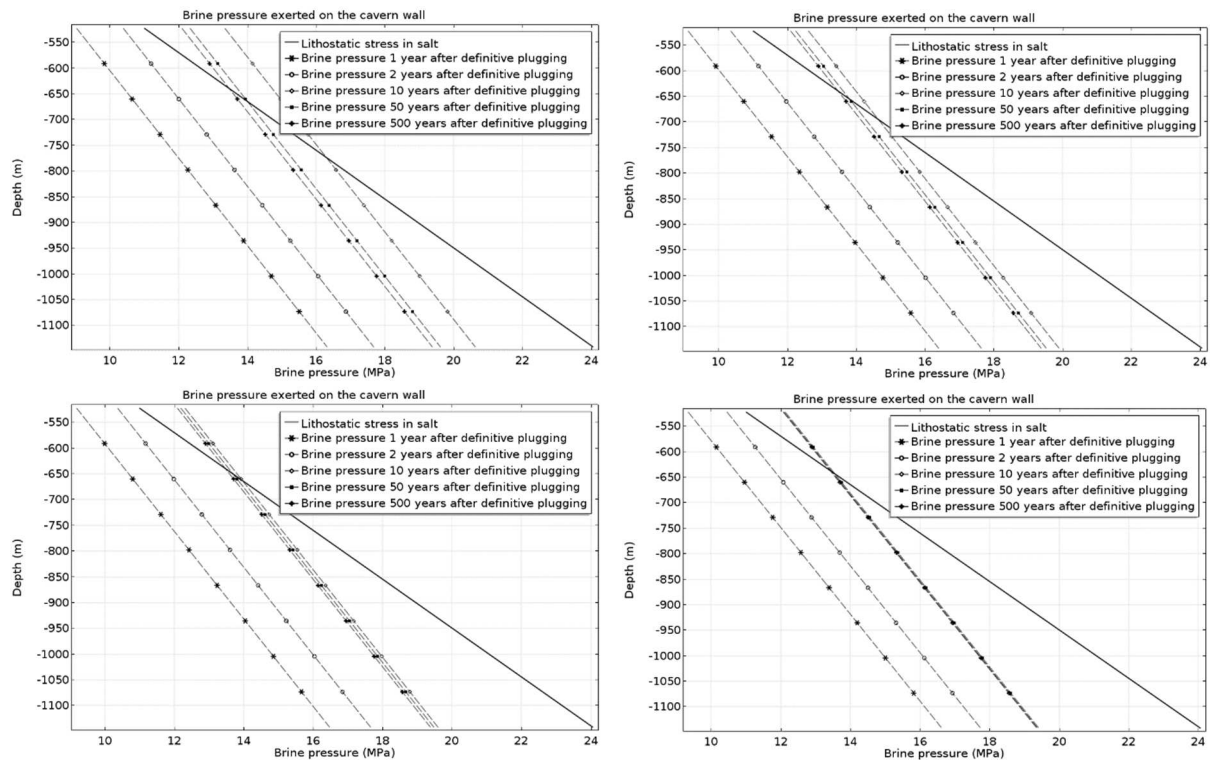


**Figure 16.** Impact of waiting time on the evolution of brine pressure exerted on the walls of cavern 26 in the 2-axi model compared to lithostatic stress within the salt.

The decrease in brine pressure after plugging, obtained by increasing the waiting time, leads to a slight increase in the Von Mises stress within the walls and the maximum plastic deformation value. All the same, in all cases, these remain very localized to the cavern's angular zones.

## 5. Conclusion

Since 1954, the Solvay company has operated, by isolated caverns, a salt diapir in the Matacões concession in Portugal (Torres Vedras region, 40 km north of Lisbon). A total of 28 caverns were created for a production of nearly 19 million tons of salt in 60 years. Solvay asked Ineris to evaluate the state of the caverns before and over the long term after abandonment.

To this end, numeric modeling was implemented, based on mining operations data and field measurements and tests (thermography, volumetry, brine purges, creep tests). Measurement analysis enabled:

- assessment of the caverns' compressibility factor and identification of possible hydraulic communications between them;
- classification of the caverns at thermal equilibrium and those that are not yet;
- determination of salt creep parameters from pressure rise measurements (between 2 purges) and well discharge measurements during creep tests. The results demonstrate some variability in the creep parameters, probably related to some heterogeneity in the salt diapir at the considered scale.

2D-axi models then allowed assessment of the caverns' current state of stability and their evolution after definitive plugging. We assessed the sensitivity of the obtained results to salt permeability ( $10^{-19}$  m<sup>2</sup> for the benchmark model) and waiting time before plugging (1 year for the benchmark model):

- if salt permeability is lower, the pressure peak will be higher and the risk of failure at the roof will be greater. We have also noticed a faster decrease of the cavern volume in this case. To the contrary, if permeability is greater, the failure risk is lower. Given its impact on predictions, it is therefore very important to determine this value precisely (abandonment tests planned for 2018 will contribute to this).
- increasing waiting time before definitive plugging will allow thermal disequilibrium to be reduced before closure and thus maximum pressure thereafter. This will lead to a reduction of failure risks

(or at least a decrease in the size of the critical zone). Moreover, the increase in waiting time could also accelerate the caverns' convergence.

The developed model was then applied to the entirety of the caverns (this was not developed in this article). We were able to show that:

- the caverns' current mechanical stability state (before the definitive plugging) is not of concern as no critical zones were identified (the salt's expansion phase threshold of 25 MPa is never exceeded, brine pressure is always well below lithostatic stress within the walls). Even when the threshold is lowered to 9 MPa, only some angular zones at the base of the caverns are concerned;
- the long-term evolution after definitive plugging demonstrates the impact in the medium term of the thermal imbalance induced by a brine pressure peak from 13 to 30 years after plugging that then slightly decreases to reach equilibrium in the long term. In the case of caverns that are already at thermal equilibrium, brine pressure evolves directly toward the value of equilibrium pressure. Overall, this long-term equilibrium pressure is relatively close to the lithostatic stress value within the salt (given our hypothesis for the permeability of salt). One observes that brine pressure exceeds (or nears) lithostatic stress near the cavern's roof for some caverns. The most critical situations are found in the most elongated or most thermally imbalanced caverns (caverns 18 and 26).

## 6. References

- [1] Bérest P., Bergues J., Brouard B., Frelat J. & Durup J.G. (1997). *Salt caverns and the compressibility factor*, S.M.R.I. Fall Meeting, El Paso.
- [2] Bérest P., Ledoux E., Legait B., De Marsily G. (1979). *Effets thermiques dans les cavités en couche salifère*, 4th Cong. Int. SIMR, Montreux, Vol.1, Balkema, pp.31-35.
- [3] Ghoreychi, M. (1992). *Synthèse des études thermomécaniques sur le sel*, document édité par G.3S à l'occasion du Conseil Scientifique de G.3S, 25 Juin 1992.
- [4] Hadj-Hassen F. (2008). *Etude de stabilité des cavités de dissolution dans les concessions de Matacaes 1 et 2 - Torres Vedras, Portugal*, Centre de Geosciences (Mines ParisTech, Armines), 37 pages, mars.
- [5] Hadj-Hassen F., Souloumiac (2011). *Etude des possibilités de développement en hauteur des cavités salines du site de Matacaes, Torres Vedras, Portugal*, Centre de Geosciences (Mines ParisTech, Armines), référence R111229/FHAD, 19 pages (annexe comprise), décembre.
- [6] Richard T. (2016). *Note de synthèse sur la constitution du SIG et du modèle géologique 3D du site d'exploitation de sel de Matacaes (Portugal)*, rapport INERIS référencé DRS-16-149164-07839A, octobre.
- [7] Thoraval A., Lahaie F. (2013). *L'abandon des cavités de stockage lessivées dans le sel : stratégies envisagées pour la fermeture des cavités et la maîtrise des aléas à long terme*, Rapport INERIS DRS-11-118134-02433B, 183 pp, août.
- [8] Thoraval A., Lahaie F., Brouard B., Berest P (2015). *A generic model for predicting long-term behavior of storage salt caverns after their abandonment as an aid to risk assessment*, International Journal of Rock Mechanics & Mining Sciences 77, pp. 44-59.
- [9] Thoraval A. (2018). *Site d'exploitation de sel par dissolution de Matakães - Modélisation géomécanique : calibrage des paramètres de fluage, évaluation de l'état actuel des cavités et de leurs évolutions à long terme*. Rapport INERIS DRS-17-149164-10228A, 85 pp, janvier.